CHEMISTRY OF MATERIALS
Article

Chem. Mater. **2009,** *21,* 2935–2940 2935
DOI:10.1021/cm9006266

Carbon-Encapsulated Metal Oxide Hollow Nanoparticles and Metal Oxide Hollow Nanoparticles: A General Synthesis Strategy and Its Application to Lithium-Ion Batteries

Jisheng Zhou,[†] Huaihe Song,*[,†] Xiaohong Chen,[†] Linjie Zhi,[‡] Shubin Yang,[†] Junping Huo,[†] and Wantai Yang[†]

[†]*State Key Laboratory of Chemical Resource Engineering, Beijing University of Chemical Technology, Beijing, 100029 P. R. China, and* [‡]*Max Planck Institute for Polymer Research, Ackermannweg 10, 55128, Mainz, Germany*

Received March 6, 2009. Revised Manuscript Received April 22, 2009

A novel and general strategy for the synthesis of carbon-encapsulated metal oxide hollow nanoparticles (HNPs) and pure metal oxide HNPs was developed from carbon-encapsulated metal nanoparticles by controlled oxidation in the air. The materials were characterized by transmission electron microscopy, scanning electron microscopy, and X-ray diffraction measurements. It was found that the morphologies and compositions of HNPs were easily tailored through adjustment of the oxidation conditions. When used as the anode materials for lithium-ion batteries, carbon-encapsulated α-Fe_2O_3 HNPs exhibit excellent cycling performance and a higher reversible capacity of about 700 mA h g^{-1} after the 60th cycle and possess great potential application in lithium-ion batteries.

Introduction

Metal oxide hollow nanoparticles (HNPs), which represent a class of intriguing materials with the unique properties of higher specific surface area, lower density, and better permeation, have widespread potential applications in many areas, including bioapplication, catalysis, lightweight structural materials, and sensors.[1] Up to now, they could be produced by various methods, of which the template-assisted approach is one of the most commonly used.[2] However, due to its complicated multistep fabricating process, this method is time-consuming, and both the yield and crystalline degree of the obtained hollow nanoparticles are low.[3] Hence, numerous efforts have been devoted to exploring template-free approaches, including Ostwald ripening,[4] electron-beam irradiation,[5] the hydrothermal method,[6] and solvothermal reaction.[7] Interestingly, the recently developed nanoscale Kirkendall-effect-assisted method[8] provides new opportunities for fabrication of metal oxide HNPs. This novel phenomenon was used by Yin and his co-workers to prepare successfully Co_3S_4 and CoO hollow nanoparticles for the first time.[8a] Since then, various hollow nanostructures, such as HNPs,[9] hollow nanowires/-tubes,[10] nanoscale-dandelions,[11] and other nanostructures[12] have been prepared via the nanoscale Kirkendall effect. However, the shells of all of the hollow nanoparticles prepared by the known procedure involving the novel effect are pure metal oxide (or pure compound) rather than hybrid material. The hybrid hollow nanoparticles have more powerful application potential.[13] In addition, in the previous studies, the

*Corresponding author. E-mail: songhh@mail.buct.edu.cn.

(1) (a) Wang, L.; Bao, J.; Wang, L.; Zhang, F.; Li, Y. *Chem. Eur. J.* **2006**, *12*, 6341. (b) Arnal, P. M.; Comotti, M.; Schüth, F. *Angew. Chem., Int. Ed.* **2006**, *45*, 8224. (c) Li, B.; Xie, Y.; Jing, M.; Rong, G.; Tang, Y.; Zhang, G. *Langmuir* **2006**, *22*, 9380. (d) Lou, X. W.; Wang, Y.; Yuan, C.; Lee, J. Y. L.; Archer, A. *Adv. Mater.* **2006**, *18*, 2325. (e) Zhao, Q.; Gao, Y.; Bai, X.; Wu, C.; Xie, Y. *Eur. J. Inorg. Chem.* **2006**, 1643. (f) Shin, J.; Anisur, R. M.; Ko, M.; K.; Im, G. H.; Lee, J. H.; Lee, I. S. *Angew. Chem., Int. Ed.* **2009**, *48*, 321.
(2) (a) Zhong, Z.; Yin, Y.; Gates, B.; Xia, Y. *Adv. Mater.* **2000**, *12*, 206. (b) Jiang, P. J.; Bertone, F.; Colvin, V. L. *Science* **2001**, *291*, 453. (c) Choi, W. S.; Koo, H. Y.; Zhongbin, Z.; Li, Y.; Kim, D.-Y. *Adv. Funct. Mater.* **2007**, *17*, 1743. (d) Titirici, M.; Antonietti, M.; Thomas, A. *Chem. Mater.* **2006**, *18*, 3808.
(3) (a) Sun, Y.; Mayers, B.; Xia, Y. *Adv. Mater.* **2003**, *15*, 641. (b) Li, L.; Chu, Y.; Liu, Y.; Dong, L. *J. Phys. Chem. C* **2007**, *111*, 2123.
(4) (a) Yang, H. G.; Zeng, H. C. *J. Phys. Chem. B* **2004**, *108*, 3492. (b) Yang, H. G.; Zeng, H. C. *Angew. Chem., Int. Ed.* **2004**, *43*, 5206.
(5) Latham, A. H.; Wilson, M. J.; Schiffer, P.; Williams, M. E. *J. Am. Chem. Soc.* **2006**, *128*, 12632.
(6) Li, L.; Chu, Y.; Liu, Y.; Dong, L. *J. Phys. Chem. C* **2007**, *111*, 2123.
(7) Wu, Z.; Yu, K.; Zhang, S.; Xie, Y. *J. Phys. Chem. C* **2008**, *112*, 11307.
(8) (a) Yin, Y.; Rioux, R. M.; Erdonmez, C. K.; Hughes, S.; Somorjai, G. A.; Alivisatos, A. P. *Science* **2004**, *304*, 711. (b) Yin, Y.; Erdonmez, C. K.; Cabot, A.; Hughes, S.; Alivisatos, A. P. *Adv. Funct. Mater.* **2006**, *16*, 1389.
(9) (a) Wang, Y.; Cai, L.; Xia, Y. *Adv. Mater.* **2005**, *17*, 473. (b) Peng, S.; Sun, S. *Angew. Chem., Int. Ed.* **2007**, *46*, 4155. (c) Cabot, A.; Puntes, V. F.; Shevchenko, E.; Yin, Y.; Balcells, L.; Marcus, M. A.; Hughes, S. M.; Alivisatos, A. P. *J. Am. Chem. Soc.* **2007**, *129*, 10358. (d) Bauer, C. A.; Robinson, D. B.; Simmon, B. A. *Small* **2007**, *3*, 58. (e) Henkes, A. E.; Vasquez, Y.; Schaak, R. E. *J. Am. Chem. Soc.* **2007**, *129*, 1896. (f) Gao, J. H.; Zhang, B.; Zhang, X. X.; Xu, B. *Angew. Chem., Int. Ed.* **2006**, *45*, 1220.
(10) (a) Fan, H. J.; Knez, M.; Scholz, R.; Nielsch, K.; Pippel, E.; Hesse, D.; Zacharias, M.; Gösele, U. *Nat. Mater.* **2006**, *5*, 627. (b) Li, Q.; Penner, R. M. *Nano. Lett.* **2005**, *5*, 1720. (c) Peng, H.; Xie, C.; Schoen, D. T.; Mcllwrath, K.; Zhang, X. F.; Cui, Y. *Nano Lett.* **2007**, *7*, 3734.
(11) Liu, B.; Zeng, H. C. *J. Am. Chem. Soc.* **2004**, *126*, 16744.
(12) (a) Yang, J.; Qi, L.; Lu, C.; Ma, J.; Cheng, H. *Angew. Chem., Int. Ed.* **2005**, *44*, 598. (b) Zhang, L. Z.; Yu, J. C.; Zheng, Z.; Leung, C. W. *Chem. Commun.* **2005**, 2683.
(13) Caruso, F.; Caruso, R. A.; Möhwald, H. *Science* **1998**, *282*, 1111.

Published on Web 05/14/2009

nanoscale Kirkendall-effect-assisted preparation of metal oxide HNPs was mostly conducted in the solution phase; for instance, Fe3O4[9b] and γ-Fe2O3[9c] hollow nanoparticles were recently synthesized in 1-octadecene and a colloidal solution, respectively. Although the direct air-oxidation conversion from bare metal nanoparticles to metal oxide HNPs was also investigated using transition electron microscopy recently,[14] it is still quite difficult to manipulate the oxidation of bare metal nanoparticles and get the desired HNPs on a large scale, because it is well-known that, when the bare metal nanoparticles are exposed to air at higher temperatures, they usually agglomerate and even spontaneously combust. The Kirkendall-effect-assisted fabrication of metal oxide HNPs on a large scale therefore faces a challenge of controlled oxidation in the air. It is essential to design a new way to further simplify the synthesis process of these interesting hollow nanoparticles and extend the potential of the nanoscale Kirkendall effect.

Herein, we construct a concept that, by creating a barrier such as carbon layers on the surface of the metal nanoparticles, the metal oxide HNPs are easily generated in the air via the nanoscale Kirkendall effect. In fact, it was confirmed that the concept is a general synthesis strategy not only for metal oxide HNPs but also for carbon-encapsulated metal oxide HNPs. A series of metal oxide HNPs such as α-Fe_2O_3, CuO, and NiO were prepared by the controlled oxidation of carbon-encapsulated metal nanoparticles (CEMNs) in the air. During the process, nanoparticles with various nanostructures and compositions, including carbon-encapsulated metal oxide (such as α-Fe_2O_3@C) HNPs and core−shell-void nanoparticles, were also facilely tailored by adjusting the oxidation temperature and time. When they were used as anode materials for lithium-ion batteries, α-Fe_2O_3 HNPs displayed better electrochemical performance than α-Fe_2O_3 solid nanoparticles, while α-Fe_2O_3@C HNPs exhibited excellent cycling performance and a highly stable and reversible capacity of about 700 mA h g^{-1} up to 60th cycle.

Experimental Procedures

Synthesis of Carbon-Encapsulated Metal Nanoparticles. Fe_3C@C nanoparticles were synthesized by cocarbonization of an aromatic heavy oil (50 g) and ferrocene (50 g) at 450 °C under autogenous pressure. The details can be seen in ref 15a. Carbon-encapsulated Ni and Cu nanoparticles were synthesized by heating a mixture of phenolic resin, Ni or Cu nitrate ($Ni(NO_3)_3 \cdot 6H_2O$ or $Cu(NO_3)_3 \cdot 3H_2O$, analytical pure grade), and hexamethylenetetramine in a metal/carbon atomic ratio of 1:16 at 700 °C for 6 h in a nitrogen gas atmosphere. The details can be seen in ref 15c.

Synthesis of Metal Oxide Hollow Nanoparticles. α-Fe_2O_3 HNPs were prepared by air oxidation of Fe_3C@C nanoparticles from room temperature to 280 °C with a heating rate of 5 °C/min and maintained at 280 °C for 24 h. Other nanoparticles with different structures and compositions were also fabricated by air oxidation at 280, 250, and 200 °C for 5 h. NiO and CuO HNPs were obtained from Ni@C and Cu@C nanoparticles, respectively, via air oxidation at 5 °C/min from room temperature to 250 °C and maintained at 250 °C for 24 and 10 h, respectively.

Characterization. The as-prepared samples were characterized using a Hitachi H-800 transmission electron microscope (TEM) operating at 200 kV. The high-resolution TEM (HRTEM) measurement was carried out with a JEOL JEM2010F microscope operating at 300 kV. The scanning electron microscope (SEM) observation was conducted on a Hitachi S-4700 field emission microscope. X-ray diffraction (XRD) was carried out with a Rigaku D/max-2500B2+/PCX system using Cu Kα radiation (λ = 1.5406 Å) over the range of 5−90° (2θ) at room temperature.

Electrochemical Measurments. The electrochemical experiments were conducted in a three-electrode system described elsewhere.[16] A working electrode was prepared by mixing an active mass (α-Fe_2O_3 or α-Fe_2O_3@C HNPs, 85 wt %), a carbonaceous additive (acetylene black, 10 wt %), and poly(vinylidene difluoride) (5 wt %), and a lithium sheet was used as both a reference and a counter electrode. A 1 M $LiPF_6$ solution in a 1:1 (volume) mixture of ethylene carbonate and dimethyl carbonate from Merck Co. was used as the electrolyte. After charge/discharge cycles, the working electrode was removed from the cell, washed with N-methyl-pyrrolidone, and then observed using HRTEM.

Results and Discussion

Scheme 1 illustrates the concept. First, carbon-encapsulated metal nanoparticles were prepared via a modified procedure reported elsewhere.[15] Through controlled oxidation in the air, the core−shell nanoparticles were converted to carbon-encapsulated metal oxide HNPs via the outward diffusion of core materials due to the nanoscale Kirkendall effect. Finally, they were completely oxidized to metal oxide HNPs accompanying the burning-off of carbon. The conversion from carbon-encapsulated Fe_3C (Fe_3C@C) nanoparticles to α-Fe_2O_3 HNPs as a special example displays this process in detail.

TEM characterization discloses that Fe_3C cores in Fe_3C@C core/shell nanoparticles with an average diameter of ca. 30 nm were encapsulated by carbon to form a core−shell structure with a shell thickness of ca. 5.5 nm (Figure 1a). Semigraphitic carbon layers[15a] encircling the cores are visible in the high-resolution TEM image (Figure 1b). XRD analysis shows that the metal core encapsulated in the carbon shell is actually Fe_3C (Figure S1, Supporting Information).

α-Fe_2O_3 HNPs were prepared by the air oxidation of Fe_3C@C nanoparticles at 280 °C for 24 h. XRD characterization demonstrates that α-Fe_2O_3 with a high crystalline structure and high phase purity was obtained (Figure 2). The weak diffraction peak that appeared at 30.16° implies the presence of trace amounts of Fe_3O_4 in the product, and the other diffraction peaks are indexed well to pure α-Fe_2O_3. The SEM image of the product (Figure 3a) shows that the obtained α-Fe_2O_3 is actually spherical nanoparticles with a smooth surface and uniform size distribution.

(14) (a) Nakamura, R.; Lee, J.-G.; Tokozaura, D.; Mori, H.; Nakajima, H. *Mater. Lett.* **2007**, *61*, 1060. (b) Nakamura, R.; Tokozaura, D.; Mori, H.; Nakajima, H. *J. Appl. Phys.* **2007**, *101*, 074303. (c) Nakamura, R.; Lee, J. G.; Mori, H.; Nakajima, H. *Philos. Mag.* **2008**, *88*, 257.

(15) (a) Huo, J.; Song, H.; Chen, X. *Carbon* **2004**, *42*, 3177. (b) Song, H.; Chen, X. *Chem. Phys. Lett.* **2003**, *374*, 400. (c) Zhao, M.; Song, H.; Chen, X.; Lian, W. *Acta Mater.* **2007**, *55*, 6144. (d) Huo, J.; Song, H.; Chen, X.; Zhao, S.; Xu, C. *Mater. Chem. Phys.* **2007**, *101*, 221.

(16) Yang, S.; Song, H.; Chen, X. *Electrochem. Commun.* **2006**, *8*, 137.

Scheme 1. Schematic Diagram of the Conversion Process from (a) Carbon-Encapsulated Metal Nanoparticles to (b) Carbon-Encapsulated Metal Oxide Hollow Nanoparticles and Finally to (c) Metal Oxide Hollow Nanoparticles

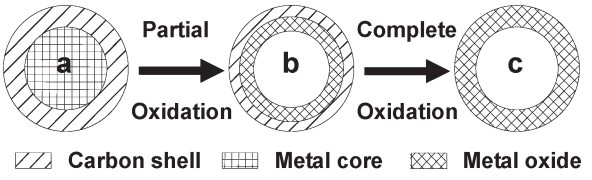

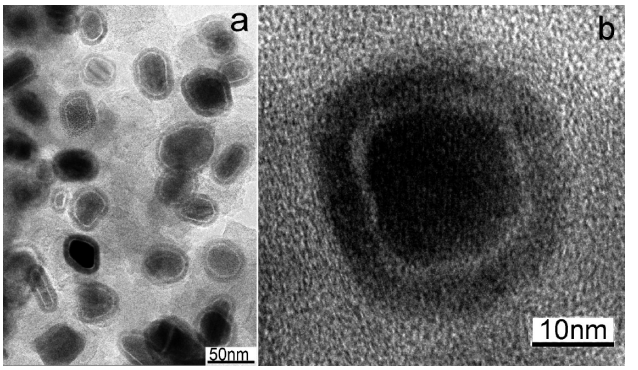

Figure 1. The low-resolution (a) and high-resolution (b) TEM images of as-synthesized Fe_3C@C nanoparticles.

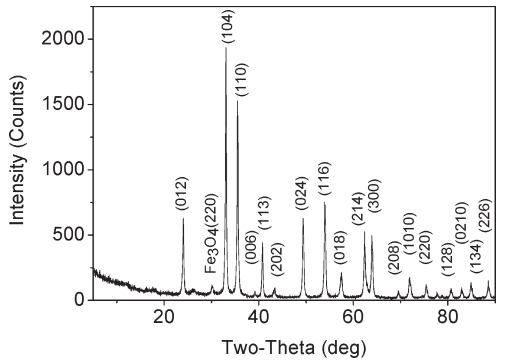

Figure 2. XRD pattern of the resulting hollow α-Fe_2O_3 nanoparticles.

Interestingly, further characterization by TEM discloses the hollow structures of these spheres (Figure 3b). The mean outer diameter of these HNPs is ca. 45 nm, and the average thickness of the shell is ca. 10 nm. HRTEM investigation shows clearly the crystalline lattices of the HNPs (Figure 3c,d). Multicrystalline shell structures with basal distances of 2.56 and 3.72 Å of the lattice are observed, which are consistent with (110) and (012) lattice spacings of hematite, respectively (Figure 3d). It should be noted that Fe_2O_3 HNPs with a single-crystalline structure are also visible frequently, as shown in Figure 3c, in which the basal distance of the lattice is 2.75 Å, corresponding to (104) in hematite. When a similar strategy was used, the other metal oxides involving CuO and NiO HNPs were also synthesized from their carbon-encapsulated nanoparticles in our laboratory (Figure S2, Supporting Information), suggesting that this approach is a general route for the bulk synthesis of metal oxide HNPs.

The carbon-encapsulated metal oxide HNPs can be fabricated facilely by adjusting the synthesis parameters.

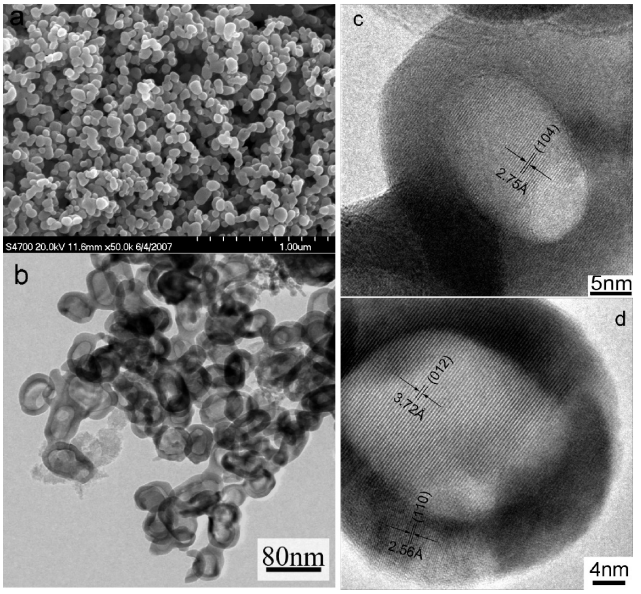

Figure 3. The morphological and structural characterizations on the final α-Fe_2O_3 hollow nanoparticles obtained by oxidation at 280 °C for 24 h in the air: (a) FSEM image, (b) TEM image, (c) HRTEM image of a single-crystalline hollow α-Fe_2O_3 nanoparticle;, and (d) HRTEM image of a single muticrystalline hollow α-Fe_2O_3 nanoparticle.

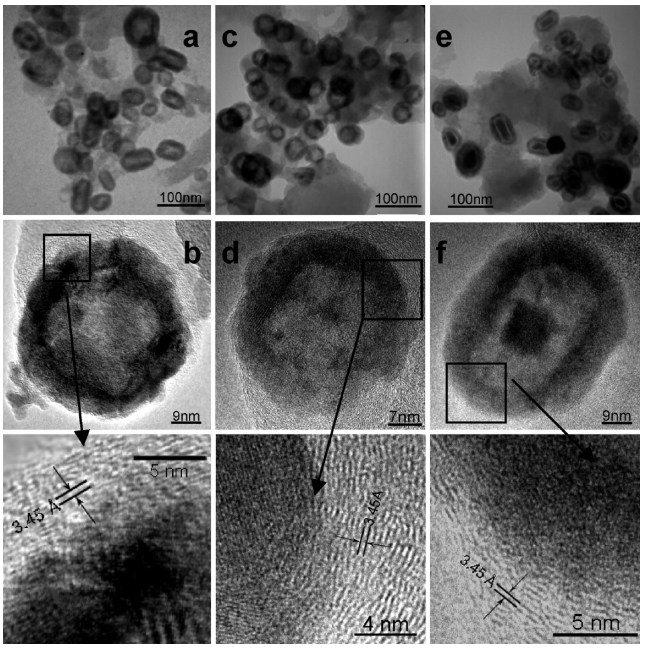

Figure 4. Nanoparticles with various structures and compositions by oxidation of Fe_3C@C nanoparticles under different conditions: (a) TEM and (b) HRTEM images of α-Fe_2O_3@C HNPs prepared at 280 °C for 5 h, (c) TEM and (d) HRTEM images of iron oxide/Fe_3C@C HNPs prepared at 250 °C for 5 h, and (e) TEM and (f) HRTEM images of core−shell-void nanoparticles prepared at 200 °C for 5 h.

Figure 4a shows that well-dispersed HNPs were prepared by oxidation at 280 °C for 5 h. The size of the HNPs with an outer diameter in the range of 30−50 nm and a shell thickness of ca. 10 nm is similar to that of pure α-Fe_2O_3 HNPs. Further, the XRD pattern (Figure S1, Supporting Information) shows that this kind of nanopaticle is composed of carbon and α-Fe_2O_3. Interestingly, HRTEM shows that the muticrystalline α-Fe_2O_3 HNPs were coated by semigraphitic carbon (Figure 4b). Therefore, the

as-synthesized nanoparticles are actually carbon-encapsulated α-Fe_2O_3 (α-Fe_2O_3@C) HNPs. The carbon content in α-Fe_2O_3@C HNPs was determined to be ca. 40.5 wt % by the removal of α-Fe_2O_3 in a HCl solution. It can be deduced that, at 280 °C, by elongating the oxidation time to the range 5−24 h, a series of α-Fe_2O_3@C HNPs with different carbon contents (in the range 0−40 wt %) can be also fabricated. At 250 °C for 5 h, the nanoparticles with complete hollow cores were formed (Figure 4c). HRTEM (Figure 4d) and XRD (Figure S1, Supporting Information) measurements confirmed that the hollow nanoparticles oxidized at 250 °C for 5 h are actually iron oxide/Fe_3C@C HNPs. When the oxidation temperature was further decreased to 200 °C for 5 h, core−shell-void structural nanoparticles with a gap of ca. 8 nm between the core and shell were generated by oxidizing Fe_3C@C nanoparticles, where the average core size shrinks to about 10 nm from the original 30 nm shown in Figure 4e. Figure 4f reveals that the single-crystal core remains in the form of Fe_3C, and the shell is composed of an inter iron and outer carbon layer, indicating that core materials diffuse into carbon shells. The XRD pattern (Figure S1, Supporting Information) shows that this kind of nanoparticle is composed of carbon, Fe_3C, and Fe_3O_4. The above observations reveal that the nanoscale Kirkendall effect directs the formation of hollow nanostructures during the oxidation of CEMNs,[8] in which the metal core diffuses faster outward than oxygen does inward. By the aid of this novel effect, it was found that other CEMNs like Cu and Ni are also converted easily to all kinds of carbon-encapsulated hollow nanostructures at various oxidation temperatures and holding hours. However, if there are no carbon shells, it is very difficult to carry out the controlled preparation of hollow nanoparticles, and hollow nanostructures cannot even form in the air due to the high activity of metal nanoparticles (Figure S3, Supporting Information). Therefore, it is reasonable to believe that the carbon shell plays important roles in this preparation. First, the carbon shell as an unbalanced interdiffusing interface of oxygen and core material can coordinate their diffusion rates during the oxidation process. Specifically, it prevents the direct contact of oxygen atoms with the metal core, avoiding their self-combustion at high temperatures. Second, due to bearing many defects,[15d] the semigraphic carbon shells can provide a large number of in-diffusing vacancies to balance the out-diffusing core materials. Furthermore, carbon layers are helpful in improving remarkably the electrochemical performance of metal oxide HNPs in the following electrochemical measurements.

It is important to clarify which kinds of factors (oxygen, heat treatment, or possible others) are driving the core materials' diffusion outward. For comparison, the as-prepared Fe_3C@C nanoparticles were heated to 280 °C and maintained at this temperature for 5 h in a pure nitrogen gas atmosphere. It was found that the nanoparticles after heat treatment remain as the original solid nanoparticles rather than hollow nanostructures (Figure S4, Supporting Information), indicating that the fast out-diffusion of core materials cannot happen only by heating in an inert gas atmosphere. Therefore, it is reasonable to believe that oxygen acts as the driving force for the out-diffusion of core materials. Electronic/ionic transport[17,9c] in the oxidation process can be employed to explain the outward diffusion of core materials in the CEMNs system. On the basis of this mechanism, oxygen atoms adsorbed onto the shell are ionized by electrons coming from the metal core. Thus, it leads to an electrical field between the metal and the shell, which will drive the outward diffusion of core materials. In addition, heating can help to accelerate the out-diffusion of core materials. Further detailed investigations on the mechanism for the diffusion of core materials are in progress.

The electrochemical properties of various carbon materials such as graphite, carbon nanotubes,[18] hard carbon spherules,[19] three-dimensionally ordered macroporous carbons,[20] mesoporous carbons,[21] and so forth used as the anode materials for lithium-ion batteries have been investigated extensively due to their high cycle stability during the Li insertion/extraction process. However, the theoretical specific capacity of graphitic carbon materials is only 372 mA h g^{-1}. In recent years, metal oxide nanoparticles (such as SnO_2,[22] Cu_2O, CoO, and NiO[23] nanoparticles) as anode materials for lithium-ion batteries, therefore, have attracted great attention because of their higher theoretical specific capacities compared with the commercial carbon electrode materials. Among these oxide nanoparticles, HNPs show more attractive electrochemical performance than solid nanoparticles,[24] owing to their hollow structures facilitating the Li^+ transport in the host matrix by providing a larger area and shorter solid-state diffusion length.[25] The iron oxide nanoparticles have also been used as anode materials for rechargeable lithium-ion batteries[26] due to their high theoretical specific capacity (ca. 1006 mA h g^{-1}),[27b] eco-friendliness, and low cost.

(17) (a) Caberra, N.; Mott, N. F. *Rep. Prog. Phys.* **1948−1949**, *12*, 163. (b) Leibbrandt, G. W. R.; Hoogers, G.; Habraken, F. H. P. M. *Phys. Rev. Lett.* **1992**, *68*, 1947.

(18) (a) Yang, S.; Song, H.; Chen, X.; Okotrub, A. V.; Bulusheva, L. G. *Electrochim. Acta* **2007**, *52*, 5286. (b) Yang, Z.; Wu, H. *Mater. Chem. Phys.* **2001**, *71*, 7.

(19) Wang, Q.; Li, H.; Chen, L. Q.; Huang, X. J. *Solid State Ionics* **2002**, *152−153*, 43.

(20) Lee, K. T.; Lytle, J. C.; Ergang, N. S.; Oh, S. M.; Stein, A. *Adv. Funct. Mater.* **2005**, *15*, 547.

(21) (a) Wang, T.; Liu, X. Y.; Zhao, D. Y.; Jiang, Z. Y. *Chem. Phys. Lett.* **2004**, *389*, 327. (b) Grigoriants, I.; Sominski, L.; Li, H. I.; Ifargan, I.; Aurbach, D.; Gedanken, A. *Chem. Commun.* **2005**, *5*, 921.

(22) (a) Han, S.; Jang, B.; Kim, T.; Oh, S. M.; Hyeon, T. *Adv. Funct. Mater.* **2005**, *15*, 1845. (b) Wang, Y.; Zeng, H. C.; Lee, J. Y. *Adv. Mater.* **2006**, *18*, 645.

(23) Poizot, P.; Laruelle, S.; Grugeon, S.; Dupont, L.; Tarascon, J. M. *Nature* **2000**, *407*, 496.

(24) (a) Lou, X. W.; Wang, Y.; Yuan, C.; Lee, J. Y.; Archer, L. A. *Adv. Mater.* **2006**, *18*, 2325. (b) Luo, J.; Cheng, L.; Xia, Y. *Electrochem. Commun.* **2007**, *9*, 1404.

(25) (a) Lee, K. T.; Lytle, J. C.; Ergang, N. S.; Oh, S. M.; Stein, A. *Adv. Funct. Mater.* **2005**, *15*, 547. (b) Wang, Y.; Su, F.; Lee, J. Y.; Zhao, X. S. *Chem. Mater.* **2006**, *18*, 1347.

(26) (a) Larcher, D.; Masquelier, C.; Bonnin, D.; Chabre, Y.; Masson, V.; Leriche, J.-B.; Tarascon, J.-M. *J. Electrochem. Soc.* **2003**, *150*, A133. (b) Hang, B. T.; Doi, T.; Okada, S.; Yamaki, J.-I. *J. Power Sources* **2007**, *174*, 493. (c) Hang, B. T.; Watanabe, I.; Doi, T.; Okada, S.; Yamaki, J.-I. *J. Power Sources* **2006**, *161*, 1281. (d) Hang, B. T.; Okada, S.; Yamaki, J.-I. *J. Power Sources* **2008**, *178*, 402.

(27) (a) Courtney, I. A.; McKinnon, W. R.; Dahn, J. R. *J. Electrochem. Soc.* **1999**, *146*, 59–68. (b) Beaulieu, L. Y.; Dahn, J. R. *J. Electrochem. Soc.* **2000**, *147*, 3237. (c) Li, H.; Shi, L.; Lu, W.; Huang, X.; Chen, L. *J. Electrochem. Soc.* **2001**, *148*, A915–A922.

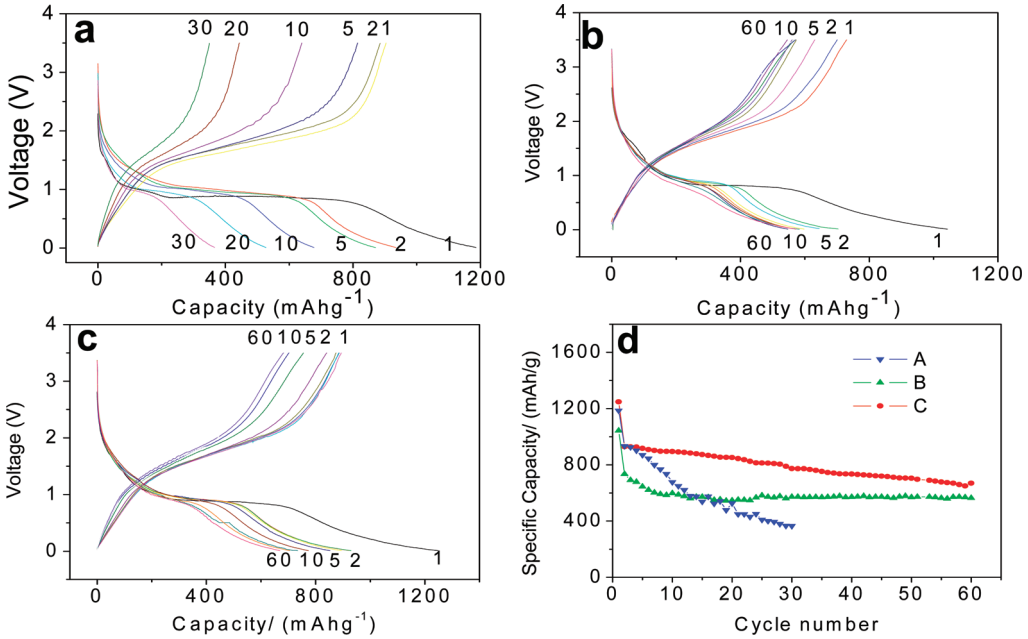

Figure 5. Charge−discharge curves of (a) α-Fe_2O_3 HNPs and α-Fe_2O_3@C HNPs with (b) 40.5 wt % and (c) 30 wt % carbon content and (d) the cycle performance of (A) α-Fe_2O_3 HNPs and α-Fe_2O_3@C HNPs with (B) 40.5 wt % and (C) 30 wt % carbon contents.

Unfortunately, a large volume change of metal oxides usually occurs during the charge and discharge processes, which leads to a decrease of cycling ability.[28] The as-prepared novel hollow nanostructure, especially with the encapsulation of carbon layers on the surface, would be expected to be ideal candidates for anode materials. Herein, their electrochemical performances as anode materials were investigated. Figure 5a shows the charge−discharge curves conducted at a current density of 0.2 mA cm^{-2} within a voltage range of 0.01−3.5 V. In the first discharge curve, two obvious plateaus (1.2−0.9 V and ca. 0.85 V) were clearly observed, which are similar to those of reported α-Fe_2O_3 solid nanostructures.[26a,28] The plateau at 1.2−0.9 V can be ascribed to the formation of cubic $Li_2Fe_2O_3$, and the 0.85 V would be attributed to the reduction from Fe^{3+} to Fe^0 and the formation of amorphous Li_2O.[28,29] From the second cycle, only one discharge slope was observed in the range of 1.2−0.85 V. The discharge capacity of the electrode in the first cycle is 1186 mA h g^{-1}, and the first Coulombic efficiency is 76%. In the second, fifth, 10th, 20th, and 30th cycles, the discharge capacities decrease gradually to about 934, 870, 678, 527, and 366 mA h g^{-1}, respectively. Nevertheless, these values are still much higher than those of the solid α-Fe_2O_3 nanoparticles. For example, it was reported recently that the capacity of the solid nanoparticles (ca. 50 nm, with 8 and 20 wt % acetylene black) tested in the voltage from 0.01 to 3.0 V at the current density of 0.20 mA cm^{-2} decreased rapidly to very small value (ca. 200 mA h g^{-1}) after the fifth cycle.[30] Compared with these solid particles, the cycling performance of as-prepared α-Fe_2O_3 HNPs improves apparently, indicating substantially that the hollow structure is helpful in mitigating the volume-change problem during the charge−discharge process to some extent.

Figure 5b shows the charge−discharge curves of α-Fe_2O_3@C HNPs with 40.5 wt % carbon tested under the same conditions as those of α-Fe_2O_3 HNPs. During the first and 60th cycles, only one discharge slope was observed in the range of 1.2−0.85 V, which is different from that of α-Fe_2O_3 HNPs. Its first discharge capacity (1042 mA h g^{-1}) is lower than that of α-Fe_2O_3 HNPs, which should be ascribed to the existence of carbon, and the first Coulombic efficiency is still up to 70%. After the 60th cycle, the reversible capacity maintains at 600 mA h g^{-1} without obvious capacity fading. If the carbon content is decreased in α-Fe_2O_3@C HNPs, the reversible capacity can be improved simultaneously. Figure 5c shows the charge−discharge curves of electrodes fabricated using α-Fe_2O_3@C HNPs with 30 wt % carbon content. This electrode exhibits a first Coulombic efficiency of 72% and a reversible capacity of 929 mA h g^{-1}. To determine the contribution of carbon in the α-Fe_2O_3@C HNPs with 30 wt % carbon content, the carbon materials after removing Fe_2O_3 using HCl were assembled electrodes and measured the electrochemical properties under the same conditions. The result (Figure S5, Supporting Information) confirmed that the reversible capacity of carbon is ca. 302 mA h g^{-1}. Thus, it can be deduced that the specific capacity from carbon is ca. 91 mA h g^{-1} (calculated by 302 × 0.3), while the specific capacity contributed by iron oxide is ca. 838 mA h g^{-1} (calculated by 929−91). Therefore, the iron oxide provides the dominant capacity in this hybrid system. Meanwhile, the reversible capacity of Fe_2O_3 in the products can be calculated to be about 1197 mA h g^{-1}, which is larger than the theoretical

(28) (a) Chen, J.; Xu, L.; Li, W.; Gou, X. *Adv. Mater.* **2005**, *17*, 582. (b) Reddy, M. V.; Yu, T.; Sow, C.-H.; Shen, Z. X.; Lim, C. T.; Rao, G. V. S.; Chowdari, B. V. R. *Adv. Funct. Mater.* **2007**, *17*, 2792.
(29) Larcher, D.; Bonnin, D.; Cortes, R.; Rivals, I.; Personnaz, L.; Tarascona, J.-M. *J. Electrochem. Soc.* **2003**, *150*, A1643.
(30) Wang, P. C.; Ding, H. P.; Bark, T.; Chen, C. H. *Electrochim. Acta* **2007**, *52*, 6650.

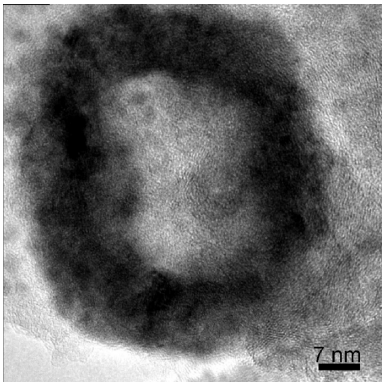

Figure 6. HRTEM image of α-Fe_2O_3@C HNPs with 30 wt % carbon content after 60 cycles in the charged state.

value of Fe_2O_3. According to the other reports,[30,31] the overfull capacity contribution should be attributed to the formation of a gel-like organic layer on the surface of hollow nanoparticles. In addition, carbon-encapsulated iron oxide hollow nanoparticles may have more locations (such as a hollow interior and defects or vacancies in the walls of hollow nanoparticles) for lithium ion storage, which should be helpful in improving the specific capacity. After the 60th cycle, the specific capacity still retains a value of 700 mA h g^{-1}. The capacity contributed by the α-Fe_2O_3 is still ca. 870 mA h g^{-1}, which accounts for ca. 86% of the theoretical capacity of α-Fe_2O_3 and is higher than the reported value (300 mA g^{-1} [30]) of solid α-Fe_2O_3 nanoparticles with adding 30 wt % acetylene black in the electrodes. Compared with the pure α-Fe_2O_3 HNPs, α-Fe_2O_3@C HNPs exhibit excellent cycling performance and a higher specific reversible capacity (Figure 5d). It is reasonable to ascribe this excellent electrochemical performance to the encapsulation of carbon and a hollow interior space. First, as the HRTEM image of the electrode material in Figure 6 shows, the nanoparticles after the 60th cycle still keep the ball-like structure and hollow interior. It indicated that the volume change and aggregation of nanosized α-Fe_2O_3 particles are hindered efficiently during the cycling process by the exterior carbon shell, which acts as both a barrier and a buffer. Second, carbon has a higher electronic conductivity.[32] In the α-Fe_2O_3@C HNPs system, as Figure 4b shows, the carbon layer and α-Fe_2O_3 connect closely, which ensures good electronic transport during the cycling process. On the basis of the above investigations, it can be concluded that the carbon-encapsulated metal oxide HNPs are appropriate and promising anode materials for high-performance lithium-ion batteries. The synthesis approach from CEMNs using controlled oxidation is a general strategy to get the desired carbon-encapsulated metal oxide hollow nanostructures. Further investigations for other metal oxide HNPs with different carbon contents are in progress in our group.

(31) (a) Rosso, M.; Brissot, C.; Teyssot, A.; Dolle, M.; Sannier, L.; Tarascon, J. M.; Bouchetc, R.; Lascaud, S. *Electrochim. Acta* **2006**, *51*, 5334. (b) Laruelle, S.; Grugeon, S.; Poizot, P.; Dolle, M.; Dupont, L.; Tarascon, J. M. *J. Electrochem. Soc.* **2002**, *149*, A627.

(32) Cui, G.; Hu, Y.-S.; Zhi, L.; Wu, D.; Lieberwirth, I.; Maier, J.; Müllen, K. *Small* **2007**, *3*, 2066.

Conclusions

In summary, a novel and general method for the preparation of carbon-encapsulated metal oxide HNPs and pure metal oxide HNPs from carbon-encapsulated metal nanoparticles was developed using controlled oxidation in the air via the nanoscale Kirkendall effect. During the oxidation process, both carbon layers and oxygen play important roles in the formation of hollow naostructures. The electrochemical measurements indicated that the α-Fe_2O_3 HNPs, especially the α-Fe_2O_3@C HNPs, exhibit excellent cycling performance and a high reversible capacity of about 700 mA h g^{-1} up to 60 cycles, when they were used as the anode materials for lithium-ion batteries. The outer carbon layers of these metal oxide HNPs are beneficial to solving the aggregation and volume expansion problems of metal oxides as a charge/discharge process. Therefore, the novel carbon-encapsulated hollow nanostructures would become a promising candidate for high-performance lithium-ion batteries.

Acknowledgment. This work was supported by the National Natural Science Foundation of China (50572003), State Key Basic Research Program of China (2006CB9326022006), and Foundation of Excellent Doctoral Dissertation of Beijing City (YB20081001001).

Supporting Information Available: XRD partterns of original Fe_3C@C naoparticles seeds and the samples by air oxidation at 200, 250, and 280 °C for 5 h; TEM images of hollow CuO nanoparticles, hollow NiO nanoparticles, and nanoparticles obtained by heat treatment at 280 °C for 3 h under the protection of flowing nitrogen; TEM and SEM images of iron oxide nanoparticles after self-combustion; and the two initial discharge/charge curves of carbon in carbon-encapsulated iron oxide hollow nanoparticles after removing the iron oxide. This material is available free of charge via the Internet at http://pubs.acs.org.